Antagonistic Functionalized Nucleation and Oxidative Degradation in Combustive Formation of Pyrene-Based Clusters Mediated by Triplet O and O<inf>2</inf>: Theoretical Study

Antagonistic functionalized nucleation and oxidative degradation in the combustive formation of pyrene-based clusters mediated by triplet O and O_2. Theoretical modelistic study.

Andrea Maranzana and Glauco Tonachini*

Dipartimento di Chimica, Università di Torino, Corso Massimo D'Azeglio 48, I-10125 Torino, Italy

Abstract.

Polycyclic aromatic hydrocarbons (PAHs) and carbonaceous nanoparticles can be oxidized right from their inception and all through their growth. Oxidation can promote their degradation too. This modelistic density functional theory (DFT) study explores in a descriptive manner if oxidation can mediate the earliest nucleation stages ("functionalized nucleation"), though contrasted by mass declension triggered by oxidation itself. An initial O (^{3}P) attack onto pyrene, chosen as representative of a generic small PAH or nascent soot lamella, forms an oxyl diradical intermediate, which can evolve to open-shell epoxide, phenol, or ketone species, or undergo mass depletion right from the beginning (without impeding further additions). Open-shell intermediates can add O or O_2 ($^3\Sigma_g^-$), and ethyne, in any order, and open the way, through formation of carbon and oxygen bridges, to addition of a second pyrene, while formation of direct carbon-carbon links between the two PAH-like parts might also occur.

Suggested running title: *C-nanoparticle oxidation/inception/degradation*

Keywords: 1) polycyclic aromatic hydrocarbons; 2) oxidation; 3) oxygen atoms and molecules; 4) soot nucleation inception; 5) density functional theory.

For the Table of Contents:

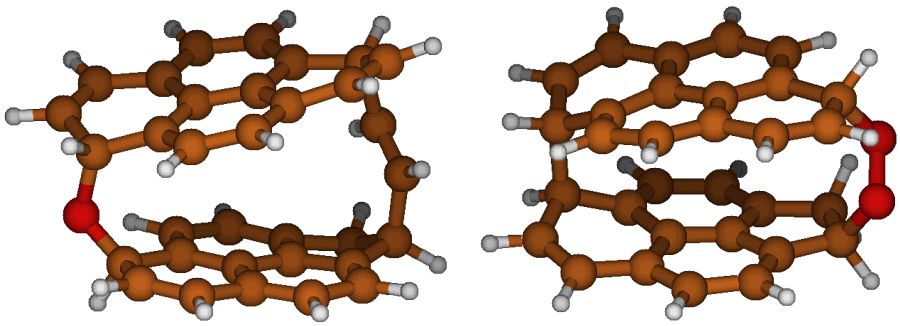

While ^{3}O and $^3O_2$ can cause PAH oxidation, they can also promote the onset of C-nanoparticle formation. But, since growth is in antagonism with CO extrusion and mass loss, the outcome of the competition is a function of T.

e-mail addresses: andrea.maranzana@unito.it; glauco.tonachini@unito.it

Introduction

Carbonaceous particulate is mostly an irregular agglomerate structure made of graphenic, PAH-like layers, or lamellae (platelets), arranged in approximately spherical shapes which further group together.[1,2] It is a significant contributor to the overall mass of atmospheric aerosol.[3,4] PAHs share the same origin and nature of soot lamellae. Their common structural traits are in fact determined by combustion processes at relatively low O_2 concentrations,[5,6] or pyrolysis.[7] Consequently, PAHs can be also found, not surprisingly, in association with soot particles.[8,9] In some studies, PAHs have been identified and quantified.[10] Carbon nanoparticles, similarly generated during combustion, can be oxidized to some extent, then can be released in the environment,. Nanoparticles (platelet clusters) can be seen both as carbonaceous particulate precursors and as primary pollutants in themselves.[11] Since the presence of a variety of functional groups affects the nanoparticle polarity and its hygroscopicity, functionalized PAHs, soot precursors, and soot spherulae are also of interest (and concern) as regards human health.[12] Some functionalizations, in addition, are known to present or enhance mutagen or carcinogenic characteristics.[6] Chemical transformations of the hydrocarbon skeleton can be pertinent to sheer PAH growth (additions of small molecules as ethyne, ring closures).[13] But they can also consist in the formation of functional groups through the reaction with a variety of small oxidants, such as ground state O and O_2 (two diradicals), O_3 (having some diradical character), NO, NO_2, and HO (all free radicals). Oxidation by these reactive species extends over the entire course of soot formation and takes place also once soot particles are emitted in the environment. It can thus accompany both molecular growth,[14,15,16,17] and condensation and/or coagulation steps of molecule-based initial systems. These processes will bring about in the end some gradual transition from relatively low-mass gas phase molecular systems to solid particles.[18] Oxidation can, on the other hand, consume carbonaceous particles, with an efficiency that depends on the combustion conditions, and in particular at higher temperatures.[19,20,21,22,23,24,25] The two processes, oxidation and mass growth (with possible soot formation), can coexist, and one can prevail over the other around some T value, T_x. Usually, at temperatures lower than T_x growth prevails over oxidation, beyond the reverse is true. If the reaction rates are reported against temperature, growing (and approximately “ ∫ -shaped”) lines are obtained for the two processes, and they cross at T_x because of their different slopes. Soot particle growth is favored at lower temperatures in fuel rich mixtures, but it can continue at higher T values if the mixture is enriched. In fact, the crossing point moves to higher T values as the fuel equivalence ratio[26] moves to higher values, i.e. from leaner to fuel-richer mixtures (see for instance Figure 1 in ref. 10, and Figure 6.7 and 6.8 in ref. 14). In principle, it can be supposed that, if a growing

hydrocarbon system can get oxidized to some extent already during the very first steps of nanoparticle inception, this could on one hand affect the basic traits of its growth mode, on the other hand put oxidative degradation in competition with growth.

Soot and PAHs have been extensively investigated under combustion conditions, and the role of oxygen examined. Soot and flame properties along the axis of a round C_2H_4/O_2/He coflow laminar jet diffusion flame were measured by Kim et al.[20,24,27] (see fig 4 of ref. 24). The soot volume fraction is shown to increase from ca. 0.5 up to more than 1.5 ppm in the region z ("height above burner") = 25-45 mm. Within the same region, O_2 and O mole fractions do not decline significantly, or even see some increase (x_{O_2} = 10^{-4} – 10^{-3} and x_O = 10^{-8} – 10^{-9}). In the same z region x_H slightly declines from 10^{-4} to 10^{-5}. Alexiou found that dioxygen addition can depress soot formation and move its peak to lower temperatures.[28] Regarding the related PAH growth, Thomas et al.[29,30] reported (for pyrolysis and fuel-rich oxidation of catechol) that an increase in dioxygen concentration has been found to boost their formation rate at temperatures lower than 1100 K, but to depress it at higher temperatures. More recently, Fuentes[31] investigated the soot formation and oxidation processes. When oxygen concentration in the oxidizer stream (O_2 + N_2) of laminar co-flow ethylene diffusion flames was varied from 17% to 35%, two regimes were observed, depending on the concentration of O_2 in the oxidized flow (oxygen index i). In the case i < 25%, soot oxidation dominates, and increases more rapidly with O_2 concentration than soot formation. When instead i > 25%, soot formation processes increase more rapidly with O_2 concentration than soot oxidation. In another recent study, these Authors found again that the soot volume fraction can be enhanced by an increase in i.[32]

Soot and PAHs have also been tentatively identified in the years in planetary atmospheres, in the envelopes of carbon-rich stars, and in the interstellar medium, hence under very diverse conditions of temperature, pressure, irradiation.[33,34,35] In extraterrestrial environments the role of atomic oxygen, in connection with the growth and presence of hydrocarbon-based systems, is problematic, and will depend on the situation considered, since (1) O can be related to their degradation, and (2) one should know its local density.[36] Then, molecular oxygen has been also detected in recent years,[37] but its coexistence with PAHs seems to be quite uncertain.

Computationally, the characteristics of the particle inception process can be investigated at different scales and by different theoretical tools.[38] In this study, quantum mechanical methods are used to model and illustrate this particular aspect: if and how nucleation could be mediated by oxidation under combustion conditions. We will also consider how oxidation can contrast nucleation by promoting PAH/soot platelet degradation. The PAH-like structures studied in our modelistic study are based on pyrene, chosen as representative of a generic small PAH or

incipient soot platelet. Pyrene has been quantified in recent studies, for instance in counterflow diffusion flames[39] and in sooting low pressure methane flames.[40]

Notwithstanding the limited size of the delocalized π–systems studied here, based on pyrene, their possible stacking is taken into account,[41] as done in our previous studies on more extended aromatic systems.[13b,42,43] Indeed, in the structures undergoing size growth upon oxidation, some stacking of the PAH-like components could be induced by van der Waals interactions, and its importance would in point of fact depend on the PAH system size.[42] In this respect, we mention that the formation of physical associations of two pyrene molecules (van der Waals complex) was recently investigated experimentally and computationally by Sabbah et al.,[44] who concluded that the rather small pyrene molecule cannot undergo a significant dimerization through van der Waals interaction at rather high temperatures. In recent studies by Kraft and collaborators,[18,38c,45] similar cases were studied. In particular, on the basis of a molecular dynamics investigation with their PAH Anisotropic Potential[46] they concluded that van der Waals pyrene dimerization is unable to contribute to soot particle formation even at low temperatures, and cannot therefore be a crucial soot formation step at flame temperatures of ca. 1500–2000 K. However, in the present study, while stacking may accompany the formation of σ–bond links between two pyrene-based structures, it does not intervene alone to keep them together.

When the functionalization and extension vs mass loss of this model hydrocarbon are here considered, they imply, following a radical addition of ground electronic state O (^{3}P) to a first pyrene, CO and HCO$^{\bullet}$ losses. These extrusions[47] form smaller radicals or diradicals, and can flank or introduce, not necessarily impede, further additions (this aspect will be discussed in section 2 and shown in Scheme 5). Then additions of O_2 ($^3\Sigma_g^-$) and ethyne can follow, and finally of a second pyrene. The mass increase steps so modeled hint to a further growth of the molecular system (nucleation), i.e. to the onset of nanoparticle formation. Data on O atom[24,48] and O_2 molecule[24,49,50] concentrations, available in the literature, depend on the experiment conditions. A limitation comes from the fact that we have chosen to restrict our study, among the variety of small reactive (di)radical oxidant species mentioned above, which could attack the PAH or PAH-like systems, to the presence of oxygen atoms and molecules, both taken in their ground electronic states (^{3}P and $^3\Sigma_g^-$, respectively).[51] One practical reason for this choice was to limit the extension of the study, which could easily become unmanageable.

Theoretical Method

The stationary (critical) points of chemical interest on the energy hypersurface are minima and first order saddle points, which correspond to stable species and transition structures (TS).

They were determined by gradient procedures[52] within the Density Functional Theory (DFT),[53] and making use of the M06-2X[54] functional. The polarized split-valence shell 6-311G(d)[55] was used in the DFT optimizations. The nature of the stationary points was checked by vibrational analysis at the same level. The energies were then recomputed by single-point energy computations with Dunning's polarized valence-3ζ cc-pV*TZ* basis set.[56]

In the case of singlet diradicaloid structures, the wavefunction stability was checked, and obtained by relaxing it in the orbital rotations space. In these cases, the spin densities expected for a diradical were obtained, instead of the "automatic" closed shell singlet solution (which obvious yields zero spin densities). Since this mixing gives a better description of the electron distribution but alters the energy, the energy values had to be consequently refined by way of Yamaguchi's formula.[57]

The 6-311G(d) thermochemical corrections gave estimates of the zero point vibrational energy (ZPE), by which the cc-pV*TZ* relative energies were corrected; the enthalpies (ΔH), entropies (ΔS), and Gibbs free energies (ΔG) were also estimated. The ΔG values reported in Schemes 1-5 (in kcal mol^{-1}), are defined with respect to the reactant reference level, i.e. $E_{ZPE}[O(^3P) + 2 \times \text{pyrene} + O_2\ (^3\Sigma_g^-) + HC{\equiv}CH]$, set to zero. They are reported as bracketed values, separated by slashes, in correspondence of a range of temperatures (T = 400/700/1500 K) which encompasses typical conditions of combustion and post-combustion (emission in the environment). In the next section, the $\Delta G^{\ddagger}$ for each step makes reference to the preceding energy minimum, while the stability of each minimum is referred to the reactants level. A Table of all forward and backwards barriers for each step can be found in the Supporting Information file.

All quantum mechanical calculations were carried out by using the GAUSSIAN09 system of programs.[58] The MOLDEN program was exploited to display some optimized structures.[59]

Results and discussion

The nascent soot platelets or PAH-like systems are modeled by involving two pyrene molecules.[60] Triplet O and O_2 attacks on one pyrene are seen as supportive of a possible addition to a second pyrene, a first step toward an incipient nanoparticle oxidized right from the beginning (we will call this “functionalized nucleation”). We attempt also to illustrate how it can be contrasted by elimination (extrusion)[47] processes which promote a mass decrease and the possible oxidation and degradation of a PAH or soot lamella. To curb an excessive expansion of our investigation, some choices have been operated regarding possible positions of addition of O and O_2 onto pyrene or reaction intermediates (with potential formation of similar regio- or diastereoisomers). The rationale about these choices[61] has been that addition will possibly involve a position of substantial spin density, but also give an intermediate geometry open to growth. In other words a geometry not presenting crowding or rigidity such to hamper a possible mass growth through addition of a second pyrene, on one side, or excessive elongation of chain structures such to prevent a robust linking of two PAH-like structures, on the other side.

An interesting aspect resides in the spin multiplicity change that subsequent attacks of triplet O and O_2 can induce, since, at some growth stage, the oxidized PAH-like system can be inclined, as a singlet, to build up not only bridges but also simple carbon-carbon bonds between two PAH-like parts.

Within an investigation plan so delineated and delimited, we will address in particular the following main issues.

(1) Assessing the extent to which steps apt to bring about various forms of oxidation can come out to be intertwined with the very early nucleation steps, through O–C and C–C connections between distinct PAH-like parts.

(2) Exploring if degradation processes, which are initiated again by oxidation, and in principle coexist with growth at some of its stages, could either alter its course significantly, or impede it altogether (in particular, mass loss via CO extrusion appears to be an interesting candidate to this role).

1. Initial steps. The reference to the reactants level [$O(^3P)$ + 2 x pyrene + O_2 ($^3\Sigma_g^-$) + HC≡CH] is generally chosen to display ΔG values in the Schemes for all critical points. Table S3 in the Supporting Information reports instead, for each reaction step, forwards and backwards Gibbs free energy barriers (which does not imply, in itself, that an equilibrium condition is attained). Initial steps (preceding possible growth) are depicted in Schemes 1-3 and discussed in subsections 1.1 to 1.3, while growth is described in Schemes 4-5, and discussed in sections 2 and 3.[62]

1.1 O(^{3}P) addition to pyrene. The first reaction step considered in all cases is the radical attack by the triplet oxygen atom onto pyrene (top left of Scheme 1).[63] A van der Waals (vdW) complex is defined, in which O interacts with the π–system.[64,65] The O radical attack onto position 1 of pyrene[66] produces the initial triplet diradical adduct ˙O–pyrene˙ labeled **A1**,[67] which is the most stable among the three possible adducts. **A1** is the starting point for our considerations. It has one unpaired electron localized on the oxyl group, and another one delocalized on the π system, and can consequently be at the origin of different reactions. Even at this early stage, the system could be open to several processes, either unimolecular, **a**–**c**, or bimolecular, **d**–**e** (Scheme 1).

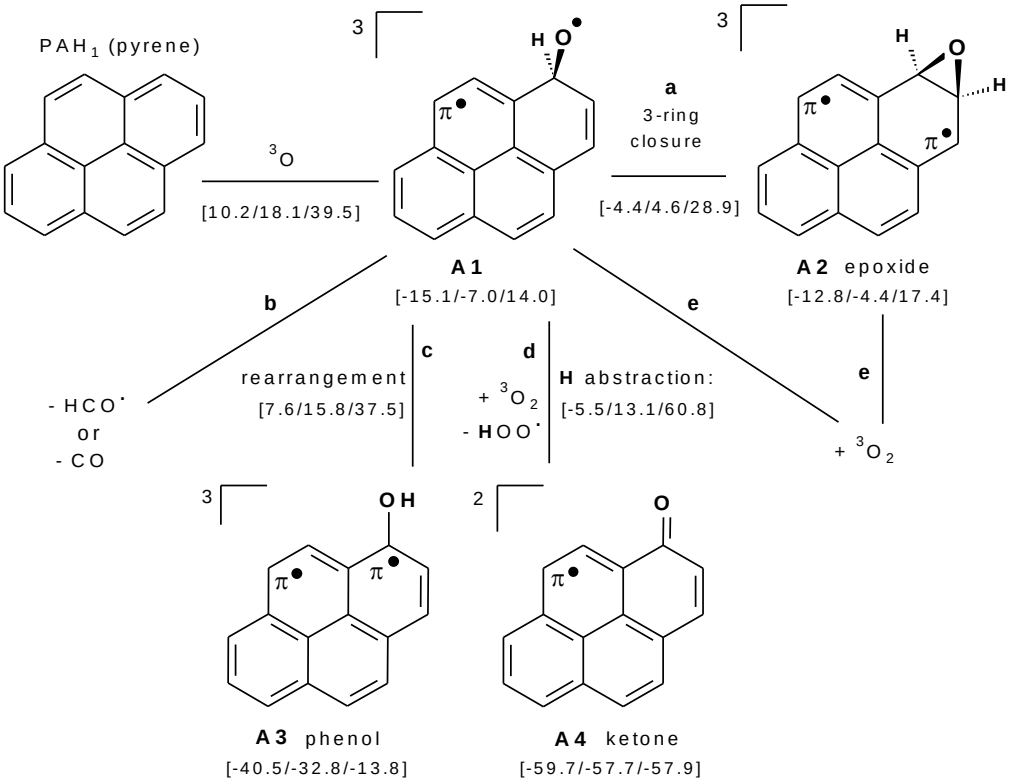

Scheme 1. Initial steps for PAH_1 (pyrene), opened by O (^{3}P) addition to give the oxyl radical adduct **A1** (here the most stable isomer is represented). (**a**) Formation of the epoxide ring of triplet **A2**. (**b**) Mass loss, described in detail in Schemes 2 and 3. (**c**) Formation of the triplet phenol diradical **A3,** via H_{gem} abstraction operated by –O˙. (**d**) H_{gem} abstraction by O_2 to give a doublet ketone **A4**. (**e**) Dioxygen addition, described in detail in Scheme S2 (Supporting Information). All systems have one π–delocalized electron; a single resonance structure is drawn. Free energy values are with respect to the reactants (ΔG at T = 400/700/1500 K between brackets; unit: kcal mol^{-1}).

(**a**) The oxyl oxygen in **A1** could reversibly close an epoxide ring to **A2**, through disruption of a π electron couple. Hence the initial oxyl/π triplet diradical becomes an all-π triplet diradical, since one π electron is used to couple with the oxyl unpaired electron to form the new σ_{OC} bond. The triplet epoxide **A2** is only some 3 kcal mol^{-1} less stable than **A1**. Hence, the backwards step (ring opening) presents a slightly lower barrier. (**b**) Next comes CO or HCO loss (extrusion), discussed in more detail in subsection 1.2, important in the oxidation and degradation of PAHs and soot

particles, which can start off from the oxyl group in **A1**. (**c**) Phenol formation proceeds through a rearrangement involving H_{gem}. This step presents a significant barrier, though it brings about an energy gain with respect to **A1** in forming the triplet π,π diradical **A3**. (**d**) O_2 abstraction of H_{gem} presents a smaller barrier with respect to **A1** and O_2. It gives the doublet ketone **A4**. The step entails a significant energy gain, but, due to the nature of the process, sees a significant temperature effect on the barrier height. (**e**) Dioxygen addition takes place by involving either the initial pyrene-O derivatives **A1** and **A2**, or the intermediates formed upon HC$^{\bullet}$O or CO losses.

1.2 Loss of HCO radical or CO. Oxidation is not only important in the degradation of fully formed soot particles, but can also cause mass diminution in an incipient carbonaceous nanoparticle or a PAH, which can take place through CO (or HCO radical) loss.[47,68]

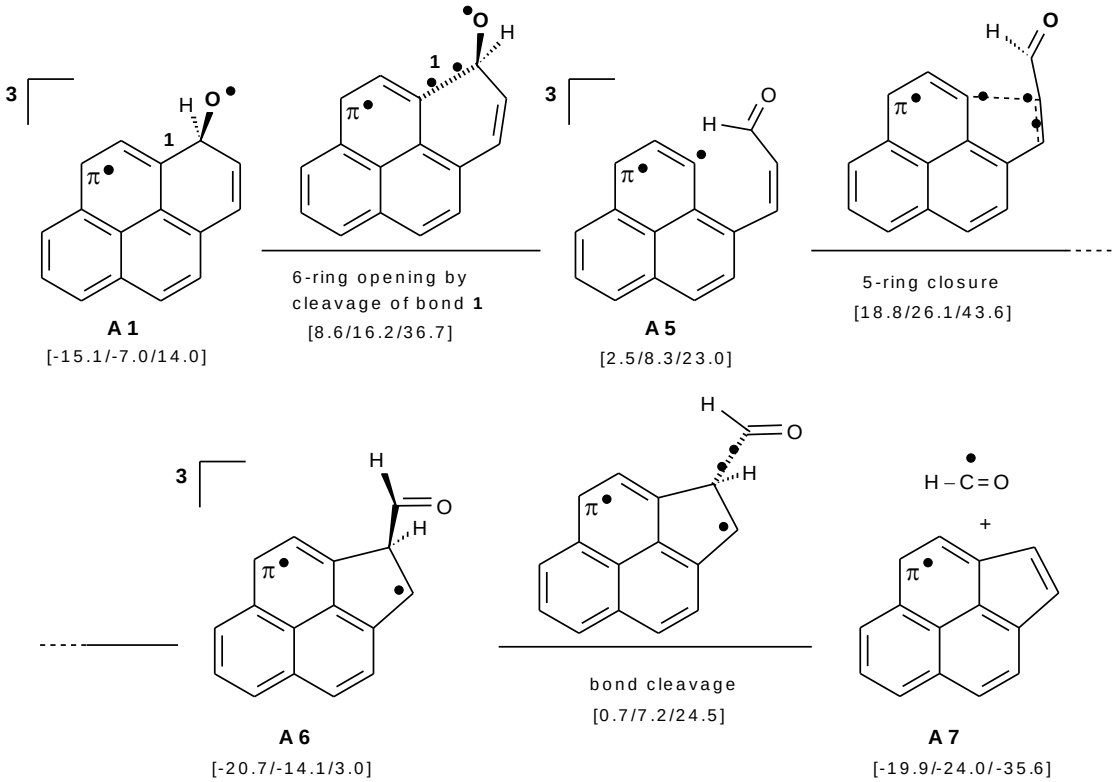

Scheme 2. Following oxidation of pyrene by atomic oxygen, loss of formyl radical (a possible precursor of CO) leaves a smaller radical PAH system, **A7**. All systems have one π–delocalized electron; a single resonance structure is drawn. ΔG values (with respect to the reactants) at T = 400/700/1500 K are between brackets; unit: kcal mol^{-1}.

In Scheme 2 it is shown that loss of a CO precursor, the formyl radical, can occur starting right from the initial oxyl radical **A1**. The overall process from **A1** to **A7** is an extrusion reaction, which does not take place concertedly, but in a few steps.[47] The cleavage of C–C bond **1** is associated to a non-negligible barrier of ca. 23 kcal mol^{-1}, fairly insensitive to T change. It leads to the diradical **A5**. The step is endoergic by ca. 17-9 kcal mol^{-1}, depending on T. A 5-ring closure presents a barrier well above the reactants level, then might generate **A6**. All these intermediates retain the triplet multiplicity. Finally, another homolytic bond cleavage (barrier ca.

21 kcal mol^{-1} high) dissociates **A6** to the formyl radical and the lighter radical PAH **A7**. Next, HC$^{\bullet}$O might lose a H atom. While the single barriers heights are, as seen, generally around 20 kcal mol^{-1} and do not depend on temperature in a marked way (that connecting **A5** to **A6** is the most sensitive), the overall sequence does depend on T, since from a single molecular system we get two: it presents a total exoergicity spanning from ca. -5 to almost -22 kcal mol^{-1}. It can also be noted that one step in particular is quite reversible (**A5** back to **A1**).

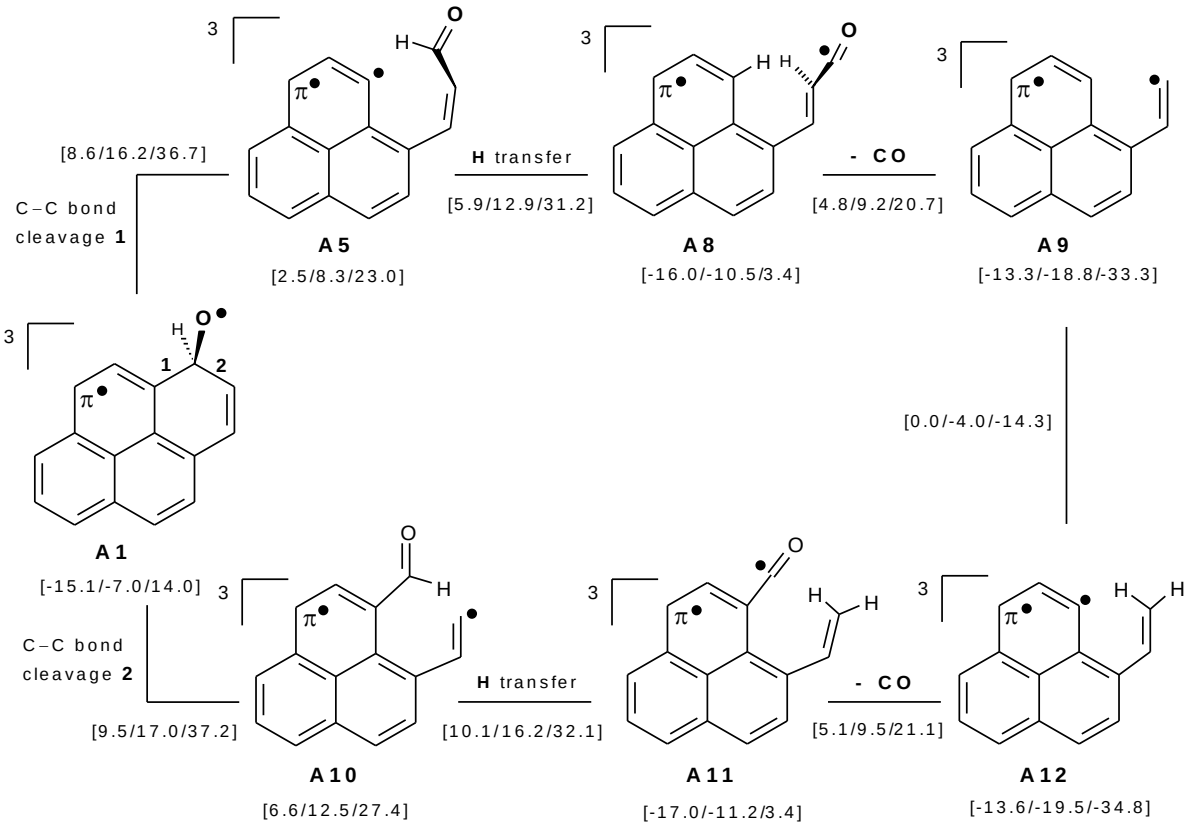

Scheme 3. CO multistep extrusions from the initial oxyl radical **A1**, leaving smaller triplet diradical PAH systems, **A9** and **A12**. **A1** undergoes two different C–C bond cleavages: **1**, to **A5** (already encountered in Scheme 2), and **2**, to **A10**. Both are followed by intramolecular hydrogen abstractions from the aldehydic groups and subsequent CO loss. All systems have one π–delocalized electron; a single resonance structure is drawn. Free energy values (with respect to the reactants) at T = 400/700/1500 K are between brackets; unit: kcal mol^{-1}.

But other transformations (Scheme 3) could depart from the **A1** intermediate, following initial homolytic openings of the O-bearing 6-ring (steps **1** or **2**). After a cleavage of the bond marked **1**, seen previously, the **A5** intermediate could undergo an intramolecular radical H abstraction (instead of the 5-ring closure just seen), i.e. a rather easy hydrogen transfer from the aldehydic group to the localized in-plane radical center, to give **A8**. The relevant barrier is ca. 8 kcal mol^{-1} high, rather insensitive to T. The reverse process has a much higher barrier. CO loss requires overcoming a barrier which is not very dependent on T, notwithstanding the formation of two species from a single one. It leaves a lighter triplet diradical, **A9**. The overall process is slightly endoergic at lower T, but becomes more and more exoergic as T rises, as expected.

The alternative cleavage of the bond marked **2** in **A1** triggers a similar sequence through **A10**[69] and **A11**. The first step shows a barrier which again varies little with T. The H transfer away from the CHO group is again not demanding (as expected on the basis of its bond strength).[70] As for the preceding H transfer case, the backwards step is more difficult. The final CO loss leaves **A12**, related to **A9** simply by a H shift. The free energies of these two intermediates are quite close, and their interconversion barrier moderately temperature-dependent.

In alternative to the above reactions, further oxidation by O_2 addition could take place in both **A1** and **A2** (steps **e** in Scheme 1 and Scheme S2 of the Supporting Information). Different additions can produce the singlet diastereomer adducts **B1**–**B4**. The reaction steps are described in detail only in the Supporting Information, section 6, where it is shown that they do not appear to be too promising.

2. Growth prepared by O_2, O, and C_2H_2 additions. The pathways described up to now bring about oxidations of the original pyrene, PAH_1, by initially forming **A1** and **A2**, then either the generation of smaller radical PAH systems (as **A7, A9, A12**) by loss of a $HCO^{\cdot}$ or CO molecule, or $C_{16}H_{10}O_3$ isomers (as **B1**–**B4**) by further dioxygen addition, which however have just been found unlikely under combustion conditions in the preceding section.[71]

We will now examine possible growth steps hopefully apt to exemplify a nucleation process under way. In any of the above cases, we choose to consider subsequent additions preferentially to high spin-density positions, either by dioxygen, (case A, Scheme 4), or, alternatively, oxygen atom (case B, primed structures, Scheme 4), and also ethyne, present, it too, with significant molar fractions in combustions.[49,49] Yet, attack to the highest spin density positions is not taken as a strict rule, as stated at the beginning of this section. O/O_2 and C_2H_2 additions are taken in any order. They end up in generating slightly larger species centered on the initial pyrene, PAH_1, which acquire, upon $^3O_2$ or ^3O addition, singlet spin multiplicity. Addition to a second PAH (PAH_2) will see peroxy (A), ether (B), and vinyl bridges binding PAH_1 to PAH_2, and will thus hint to nucleation (Scheme 5).

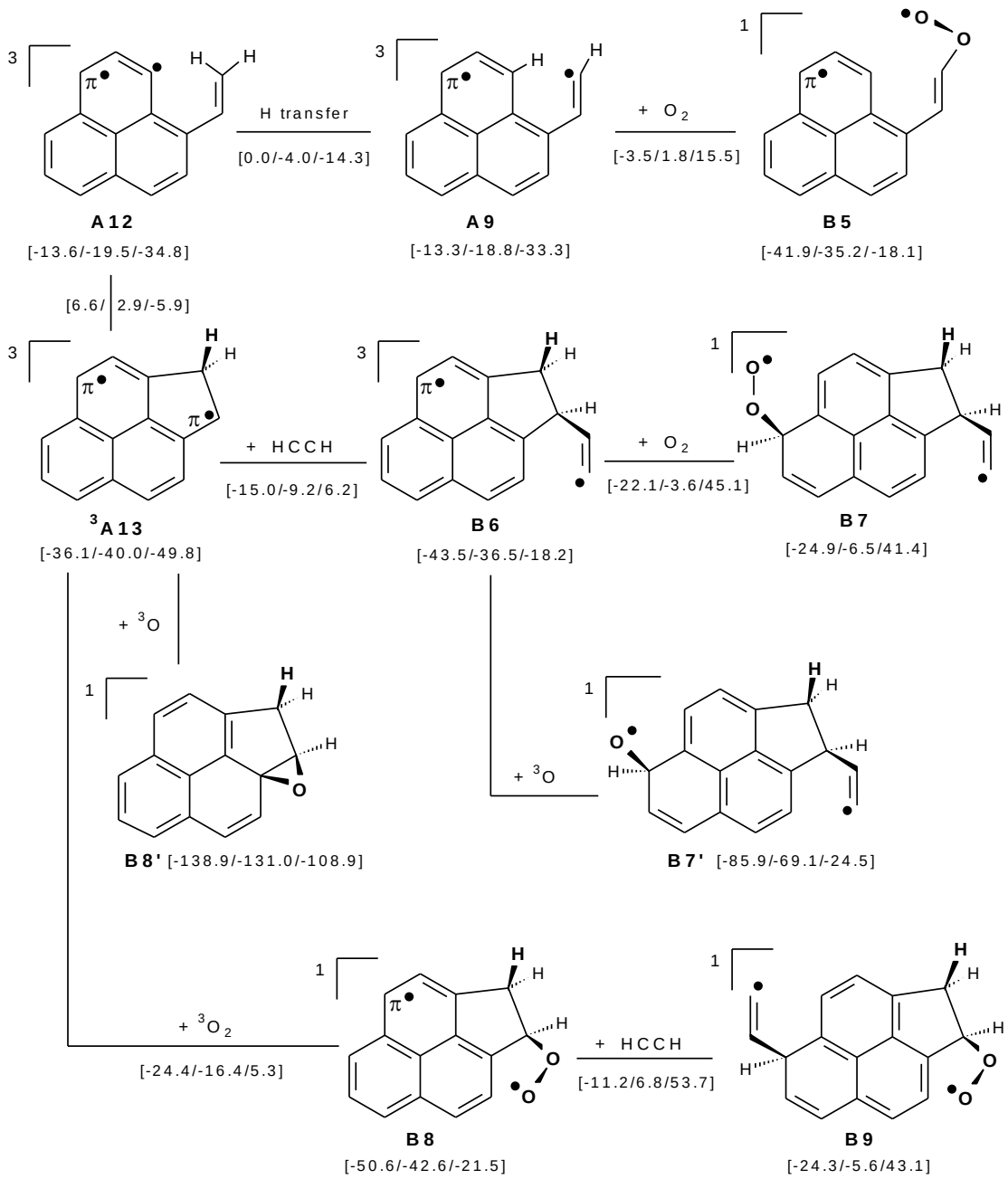

Scheme 4. Oxidation / addition steps by dioxygen (case A), oxygen atom (case B) and ethyne, in any order, starting from the triplet diradicals **A9** or **A12** seen in Scheme 3. All systems have one π–delocalized electron; a single resonance structure is drawn. Free energy values are with respect to the reactants (ΔG at T = 400/700/1500 K between brackets; unit: kcal mol^{-1}).

The triplet diradical **A12** (CO loss product encountered in Scheme 3), is connected to **A9** by a simple H shift. Also a 5-ring closure can occur in **A12**, in particular, to give the π diradical **A13**, similar to another mass-loss product, the radical **A7** of Scheme 2. In **A13** the unpaired electrons (triplet state) are both pertaining to the π system, but while one is delocalized on the three fused 6-rings, the other is localized in one position of the 5-ring, as shown.[72] Ethyne, dioxygen, or oxygen atom additions to **A9**, **A12**, or **A13** can be involved in further reaction steps shown in Scheme 4. The structures **Bn** (dioxygen attack) and **Bn'** (O atom attack) are thus formed. The additions are privileged if occurring onto the site of a localized unpaired electron: (**1**) the in-plane sp^2 site in **A12** (top ring, spin density of 1.28), (**2**) the vinyl position for **A9** (spin density of 1.28),

and (**3**) the p orbital site on the 5-ring in **A13** (spin density of 0.93). Also addition to positions belonging to the delocalized π system, and having lower spin density, will be contemplated, since they allow the presence of two peripheral substituents in appropriate positions, which can prepare the scene for the formation of strong PAH_1-PAH_2 connections. Will now examine in more detail the three possibilities just declared.

(**1**) Though additions can take place involving a ring sp^2 radical site, the resulting substituent groups must result rather rigidly bound. This possibility has been examined for **A12**, and this rigidity causes the group to be inclined to lie mostly on the plane approximately defined by PAH_1. These were obviously deemed not promising because we looked for structures extended in the three dimensions, in other words to subsequent formation of heavier "nuclei" made by not simply lined parts.[73]

(**2**) Dioxygen addition (case A) to the vinyl site of **A9** might produce **B5**, a singlet intermediate bearing a –CH=CH–OO chain, with a terminal radical site. When considering the forward and backwards processes centered on **A9**, we see that since **A9** and **A12** are almost isoergic at any temperature, the two related barriers are of course very close. The barriers for the **A9**-**B5** bimolecular step, [9.8/20.6/48.8] kcal mol^{-1}, are to be compared (a) again with those of the **A9**-**A12** backwards step, and then (b) with those of the unimolecular **B5**-**A9** backwards step, [38.4/37.0/33.6], in which dioxygen loss results less sensitive to T variations. At the two lower T values, dioxygen addition seems easier than its re-dissociation, but only at T < 500 K **B5** formation is easier than the step back to **A12**. Moreover, though a further PAH_2 addition to this site in **B5** is possible, we have also to consider that in this singlet system a unimolecular process, the 7-ring closure, will compete with it efficiently (see the Supporting Information, section 7).

(**3**) Turning now to triplet **A13**, it could add either ethyne or dioxygen to the 5-ring site with significant spin density. Both additions are considered. Ethyne addition would give **B6**, and upon a subsequent O_2 addition the singlet **B7** diradical would form. When considering the forward and backwards processes centered on **B6**, we see that for the **A13**-**B6** step the *G* barriers are [21.1/30.8/56.0] kcal mol^{-1}, to be compared with those for the **B6**-**A13** backwards step, [28.5/27.3 /24.4]. Beyond 600 K, the backwards step is easier. Then, for the **B6**-**B7** bimolecular step, the barriers are to be compared with that of the unimolecular **B7**-**B6** backwards step. Dioxygen loss (again little sensitive to T variations) results much easier than its addition at all temperatures. Due to this last set of data **B7** formation is quite unlikely.

Similarly, but in the reverse order, a first O_2 addition to **A13** would give the singlet diradical **B8**. We consider now the forward and backwards processes centered on it. For the **A13**-**B8** step the G barriers are lower than those for the **B8**-**A13** backwards step at the two lower temperatures. The backwards step is easier only at 1500 K, and up to ca. 800 K the pathway

passing through **B8** could be open to further PAH_2 addition. We will consider possible growth steps from **B8** in the next subsection. If ethyne addition instead follows, it gives **B9.** But the barriers for the **B8**-**B9** bimolecular step result all higher than the **B8**-**A13** backwards barriers. The formation of **B9** seems thus precarious.

As an alternative to the above dioxygen additions, an O atom could be involved.[24,48,65] We will consider, to illustrate this possibility, only the steps departing from **A13**, avoiding the formation of longer chains, as was the case for **B5**. Again, O addition will be taken as occurring either after or before an ethyne addition. Of the imaginable structures, **B8'** comes out not to be a singlet diradical but a very stable closed shell epoxide.[74] **B7'** (from O addition to **B6**) could instead, as a diradical, add a second PAH. This structure is attained very easily, through a barrierless and exceedingly steep all-downhill pathway on the energy surface. Though the attack is one out of some more or less equivalent attacks on positions of relatively high spin density, we proceed further from one single position.

3. Growth through PAH_2 addition. The additions shown in Scheme 4 create singlet PAH-like intermediates with side chains that bear unpaired electrons (**B7'**, **B8**). They prepare the scene for a possible further PAH_2 addition, which exemplifies the beginning of a nucleation process. Scheme 5 illustrates two growth possibilities. Starting from **B7'**, the first attack can be carried out on PAH_2 by either of the two high-spin-density positions (the oxyl oxygen or the terminal vinyl carbon). Then the other can form a second bridge between the two PAH-like parts. Whichever the choice, the cage-like structure **C2** is obtained. We have selected in Scheme 5 the choice "vinyl first, then oxygen".

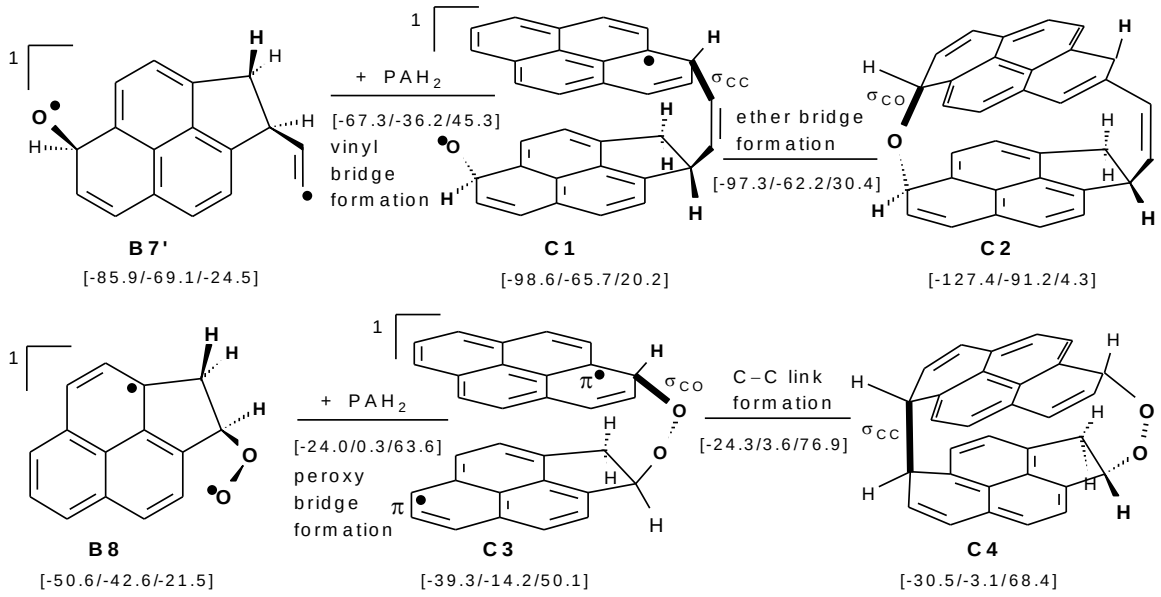

Scheme 5. Further pyrene (PAH_2) addition steps, which describe nucleation inception through formation of closed shell adducts. The PAH-like parts are bound by vinyl and peroxyl bridges, or directly through σ_{CC} bonds. Free energy values are both with respect to the reactants (ΔG at T = 400/ 700/1500 K between brackets; unit: kcal mol^{-1}). A side view is chosen for the adducts (new bonds in bold).

The barrier for the **B7'**-**C1** step is [18.7/32.9/69.8] kcal mol^{-1} high. The reverse step requires overcoming a barrier of [31.3/29.5/25.1] kcal mol^{-1}. This datum would indicate that **C1** could form at the lower temperatures, but less and less easily beyond 700 K. This temperature could be seen as a threshold, beyond which the addition process cannot be efficient. But the second barrier, to get **C2** from **C1**, is of very moderate height. They can be compared and formation of **C2** appears to be feasible.

A different connection is obtained when starting from **B8**, in which a single peroxyl substituent can potentially link PAH_2. In this case, the energetics is less favorable. The *G* barrier for the **B8**-**C3** step is high. The reverse step **C3**-**B8** requires overcoming a lower barrier. However, it can be contrasted with the **C3**-**C4** step. Though the barrier to get **C4** from **B8** puts this step on a favorable ground at the lowest T, it is not so at the two higher T values. Therefore, **C4** unlikely forms but at the lowest temperature, approximately not beyond 500 K. In summary, while **C2** might form more easily, especially at lower T, **C4** formation is not as feasible. The steps leading to these rather compact structures (Figure 1) can be seen as more or less viable examples of nucleation onset. But, within the limits of our growth exemplification based only on pyrene elementary units, we have to stress at this point that the formation of heavier systems containing two pyrene units, taking place through a σ–bridging promoted by oxygen and ethyne, is viable only at rather low temperatures.

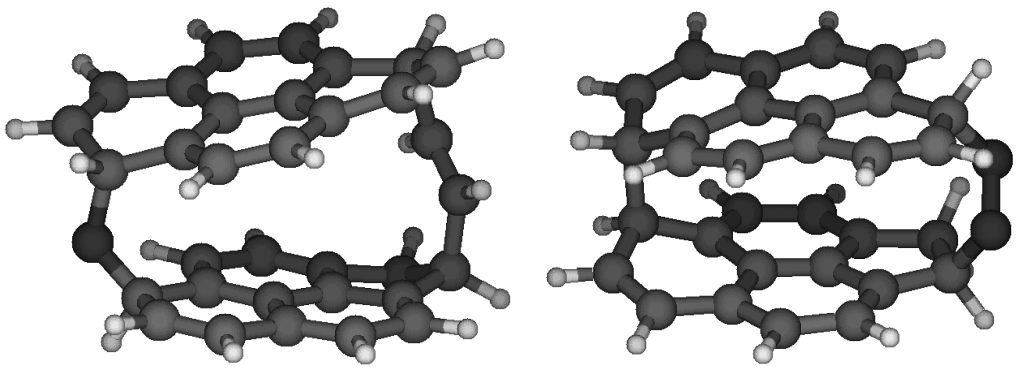

C2 **C4**

Figure 1. Two closed shell addition products shown in Scheme 6, in which the PAH-like parts are bound either by ether and vinyl bridges (**C2**), or by a peroxyl bridge, right, and directly through a σ_{CC} bond, left (**C4**).

In all singlet peroxyl species considered so far, ring closure to a peroxide intermediate or formation of a peroxy linkage between PAH-like moieties, can in principle take place. On the other hand, the relatively weak peroxy bond, however formed, might undergo cleavage, with

formation of two oxyl radical functionalities and possible mass loss. These steps are described in detail in the Supporting Information, section 7.

The succession of reaction steps described so far provides an obviously incomplete illustration of the possible interconnection between oxidation processes which give simple functionalization, mass declension via CO loss, or oxygen-mediated nucleation. Within the limits of our exemplification, we can now recall the issues raised at the beginning of this section, and state the following points. **(1)** At temperatures < 700 K, oxidation can give a chance of growth, through the formation of peroxidic and aliphatic connections (e.g. –CH=CH– bridges) between PAH-like parts, or sheer C–C connections between them that involve carbons belonging to the initial PAHs. **(2)** Mass loss can certainly take place, yet cannot impede successive growth modes, just as oxidation following growth can cause, by contrast, mass loss via CO extrusion. The two processes can coexist, and appear, from a mechanistic point of view, to be deeply intertwined: the balance between mass growth and degradation will ultimately depend on the combustion conditions.

These results can be compared with the conclusions previously drawn in the experimental and theoretical study by Sabbah et al.,[44] who ruled out the possible formation of van der Waals pyrene dimers at combustion temperatures. Our results can also be compared with some recent theoretical investigations. Those by Kraft and coworkers[18,38c,45,46] took into account the possible stacking of larger PAH units via van der Waals interaction, and found that pyrene dimerization is unlikely as a critical soot formation step for T ≈ 1500-2000 K. Then also the studies by Violi and coworkers,[75] who discuss also the role of side chains on the PAH propensity to dimerize. They find that for T ≥ 1000 K, only large PAHs see the formation of dimers favored over the free monomers, ruling out the simple stacking of pyrene as the main step for soot formation.[76] In this respect, we can recall that a van der Waals pyrene dimerization had been considered in preceding years as a possible seed for soot nucleation.[77]

Conclusions

The nucleation onset of a carbonaceous nanoparticle in an oxidizing environment has been examined by theoretical modeling, using density functional theory (DFT). This work has been set to illustrate the possible interconnection modes of PAH or soot platelet oxidation by ^3O and $^3O_2$ with mass growth (involving also ethyne) and, by contrast, with their degradation. Our purpose was a qualitative representation of the events which involve a pyrene-based system, not

comprehensive of all conceivable reaction pathways, aimed to clarify: (1) if the very first nucleation steps can be mediated by oxidation (a process here dubbed "functionalized nucleation"); then (2) to get some answer regarding the question if processes that cause mass loss can also impede growth steps.

The reaction pathways have been examined, and the relevant thermochemistry defined at different combustion or post-combustion temperatures (from T=1500 K down to 700 and 400 K). The functionalization, mass loss, or extension of the initial system imply: σ_{CO} and σ_{CC} bond formations, σ_{OO} bond cleavages, CO and $HCO^{\bullet}$ losses (extrusions), H transfers, as well as a more or less pronounced stacking of the aromatic components. Succeeding O and O_2 radical attacks on PAH systems can oxidize them by forming oxygen-containing functional groups. Phenol, ketone, epoxide, ether, and peroxide functionalities can be present in the open shell intermediates, aside to oxylic and peroxylic radical groups. Meanwhile, when oxyl radical groups form, extrusion of CO (or $HCO^{\bullet}$, seen as a CO precursor) can bring about mass loss. These losses alter the intermediate structures by forming smaller hydrocarbons of radical or diradical nature, but do not inhibit further O_2 or hydrocarbon (ethyne was considered here) additions and growth. Then, one or the other of the antagonistic growth and depletion phases can become the dominant process, depending on temperature. The subsequent radical attacks open the way to addition to another PAH, with formation of –O–, –O–O–, and –CH=CH– bridges between PAH-like parts. They can also induce singlet spin multiplicity and formation of direct –C–C– links between the PAH-like parts (Scheme 5). Whichever the connection, the "PAH-linkup" structures so formed (efficiently only up to ca. 700 K) can be seen as the seeds of carbon nanoparticle nucleation, since they could proceed towards a mass increase through further radical reactions, then by physical processes of coagulation and condensation.[78]

Within the limits of our model, we can conclude that the formation of more extended molecular systems, with two pyrene units σ–connected by oxygen and vinyl spacers, is possible only at rather low temperatures. If PAHs significantly larger than pyrene were considered, a twofold effect could be present. (1) A larger dispersion effect could promote the formation of van der Waals complexes, as observed for instance in refs 42 and 45; it could as well enhance van der Waals interactions and consequent stabilization in intermediates already bound by σ–bridges. (2) A larger size might bring about some extra flexibility in the PAH-like units, and consequently a smaller deformation energy for each PAH-like unit upon σ–linking, since the deviation from the ideal planarity could be distributed over a larger number of carbons, thus easing the formation of σ–bond connections between them.[43]

From the features of the simple reaction pathways investigated, a qualitative description emerges, where functionalization (oxidation) of PAH molecules, and formation of oxygen and

carbon links between PAH-like components, can be significantly interconnected. They can also coexist with mass loss steps, and the two channels will bear different relative importance depending on temperature.

In summary, this study provides a qualitative but interesting result: During combustion, while ^3O and $^3O_2$ additions can cause various forms of PAH oxidation, they can also trigger, contextually, the growth of a carbon-based nanoparticle. The computational modelistic results suggest that mass growth can most likely occur by this oxygen intermediacy at lower temperatures, while at higher temperatures extrusion can prevail, and bring about mass loss.

Acknowledgments

This work was conducted in the frame of EU ACCENT–PLUS (Atmospheric Composition Change, the European NeTwork of Excellence).

Supporting Information. The supplementary material for this article includes the geometries and energetics of all optimized structures, spin densities for selected structures, and a table with all free energy barriers.

References and notes

1 See for instance: N. P. Ivleva, A. Messerer, X. Yang, R. Niessner, U. Pöschl, *Environ. Sci. Technol*. **2007**, *41*, 3702-3707, and: http://www.ws.chemie.tu-muenchen.de/groups/director projects0 /raman-soot/.

2 J.-O. Möller, D. S. Su, R. E. Jentoft, U. Wild, R. Schlögl *Environ. Sci. Technol*., **2006**, *40*, 1231-1236.

3 W. F. Cooke, J. J. N. Wilson, *J. Geophys. Res.* **1996**, *101*, 19395-19409.

4 C. Liousse, J. E. Penner, C. Chuang, J. J. Walton, H. Eddleman, H.Cachier, *J. Geophys. Res.* **1996**, *101*, 19411-19432.

5 K.-H. Homann, *Angew. Chem. Int. Ed.* **1998**, *37*, 2434-2451.

6 B. J.; Finlayson-Pitts, J. N., Jr. Pitts, *Chemistry of the Upper and Lower Atmosphere*; Academic Press, New York, **2000**, ch. 10.

7 See for instance: H. Böhm, H. Jander, *Phys. Chem. Chem. Phys.* **1999**, *1*, 3775-3781. E. B. Ledesma, M. A. Kalish, P. F. Nelson, M. J. Wornat, J. C. Mackie, *Fuel* **2000**, *79*, 1801-1814. I. Naydenova, P. A. Vlasov, J. Warnatz, *Proc. Eur. Comb. Meeting* **2005**. C. Jäger, F. Huisken, H. Mutschke, I. Llamas-Jansa, Th. Henning, *Astrophys. J.* **2009**, *696*, 706-712. C. Jäger, H. Mutschke, F. Huisken, S. Krasnokutski, A. Staicu, Th. Henning, W. Poppitz, I. Voicu, *Astrophys. J. Suppl.* **2006**, *166*, 557-566.

8 U. Pöschl, T. Letzel, C. Schauer, R.Niessner, *J. Phys. Chem. A* **2001**, *105*, 4029-4041.

9 R. M. Kamens, J. Guo, Z. Guo, S. R. McDow, *Atmos. Environ*. **1990**, *24A*, 1161-1173.

10 See for instance: J. Y. Hwang, S. H. Chung *Comb. Flame* **2001**, *125*, 752–762.

11 K.-H. Kima, S. A. Jahan, E. Kabir, R. J. C. Brown *Env. Int.* **2013**, *60*, 71**–**80.

12 L. A. Sgro , A. Simonelli, l. Pascarella, P. Minutolo, D. Guarnieri, N. Sannolo, P. Netti, A. D'Anna, *Environ. Sci. Technol.* **2009,** *43,* 2608–2613.

13 We have for instance studied by similar theoretical tools the growth of an aromatic system involving small alkynes either by the radical-breeding mechanism in the gas phase: (a) A. Indarto, A. Giordana, G. Ghigo, G. Tonachini, *J. Phys. Org. Chem.* **2010**, *23*, 400-410, or by a HACA mechanism when adsorbed on a model soot platelet: (b) A. Indarto, A. Giordana, G. Ghigo, A. Maranzana, G. Tonachini, *Phys. Chem. Chem. Phys*. **2010**, *12*, 9429–9440.

14 J. F. Griffiths, J. A Barnard, *Flame and Combustion*, Blackie Academic and Professional, **1995**, § 6.8, in particular: pp 117 and 118. The crossings in Figure 6.7 are related to the bell-shaped soot yield curves, as a function of T, which are observed oftentimes (see ref. 23 Ch. 18, in particular pp 294 and 295).

15 H. S. Homan, *Comb. Sci. Tech.* **1983**, *33*, 1-15.

16 N. E. Sánchez, A. Callejas, Á. Millera, R. Bilbao, M. U. Alzueta *Energy & Fuels* **2013**, *27*, 7081-7088.

17 J. Xi, B.-J. Zhong *Chem. Eng. Technol.* **2006**, *29*, 665-763.

18 D. Chen, T. S. Totton, J. Akroyd, S. Mosbach, M. Kraft *Carbon* **2014**, *77*, 25–35.

19 A review on soot oxidation: B. R. Stanmore, J. F. Brilhac, P. Gilot, *Carbon* **2001**, *39*, 2247-2268.

20 F. Xu, A. M. El-Leathy, C. H. Kim, G. M. Faeth, *Comb. Flame* **2003**, *132*, 43–57.

21 On soot gasification by O_3 and NO_2: S. Kamm, H. Saathoff, K.-H. Naumann, O. Möhler, U. Schurath, *Comb. Flame* **2004**, *138*, 353-361.

22 For comparison, we mention some DFT studies modeling gasification. A. Montoya, F. Mondragòn, T. N. Truong *Fuel Proc. Tech.* **2002**, *77–78*, 125-130. J. F. Espinal, A. Montoya, F. Mondragòn, T. N. Truong *J. Phys. Chem. B* **2004**, *108,* 1003-1008. A. Raj, G. R. da Silva, S. H. Chung *Comb. Flame* **2012**, ***159***, 3423-3436.

23 J. Warnatz, U. Maas, R. W. Dibble *Combustion*, 4th edition, Springer Verlag **2006** (Chapter 18, pp 282-296).

24 C. H. Kim, F. Xu, G. M. Faeth, *Comb. Flame* **2008**, *152*, 301–316. Mole fraction ($\varkappa$) profiles are reported, in particular for O and O_2, as a function of *z,* the "height above burner" parameter, and pressure P (see Figures 4-7). They were determined in laminar jet nonpremixed flames (C_2H_4–He mixtures in an oxygen/helium coflow) at P = 1.0–8.0 atm.

25 I. Glassman, R. A. Yetter, *Combustion*, 4th edition, Elsevier, **2008** (Chapter 8.E, in particular §3).

26 In a combustion (flame), the 'air equivalence ratio' λ is defined as $\lambda = (x_{air}/x_{fuel})/(\varkappa_{air}/\varkappa_{fuel})$, where x and $\varkappa$ denote mole fractions. In particular, the $\varkappa$'s are the stoichiometric mole fractions, i.e. those for which fuel and oxidizer consume each other completely. The 'fuel equivalence ratio' Φ is just the reciprocal of λ. It follows that for $\Phi=\lambda=1$ we have a stoichiometric combustion; for $\Phi>1$ and $\lambda<1$ we have a rich combustion (excess of fuel); for $\Phi<1$ and $\lambda>1$ we have a lean combustion (excess of oxidizer). See for instance ref. 23.

27 C.H. Kim, A.M. El-Leathy, F. Xu, G.M. Faeth, *Comb. Flame* **2004**, *136*, 191–207.

28 A. Alexiou, A. Williams Comb. Flame **1996**, *104*, 51-65.

29 S. Thomas, E. B. Ledesma, M. J. Wornat *Fuel* **2007**, *86*, 2581–2595.

30 S. Thomas, M. J. Wornat *Fuel* **2008**, *87*, 768–781.

31 A. Fuentes, R. Henríquez, F. Nmira, F. Liu, J. L. Consalvi *Comb. Flame* **2013**, *160*, 786–795.

32 R. Henríquez, R. Demarco , J. L. Consalvi , F. Liu, A. Fuentes *Comb. Sci. Tech*., **2014**, *186*, 504-517.

33 A. G. G. M. Tielens, *Rev. Mod. Phys*., **2013**, *85*, 1021-1081.

34 M. Agúndez, V. Wakelam, *Chem. Rev*., **2013**, *113*, 8710-8737.

35 S. E. Malek, J. Cami, J. Bernard-Salas, *Astrophys. J.,* **2012**, *744*, 16-24. C. Boersma, C. W. Jr. Bauschlicher, A. Ricca, A. L. Mattioda, E. Peeters, A. G. G. M. Tielens, L. J. Allamandola, *Astrophys. J*., **2011**, *729*, 64-78. J. M. Bakker, B. Redlich, A. F. G. van der Meer, J. Oomens, *Astrophys. J*., **2011**, *741*, 74-83.

36 A. Occhiogrosso, S. Viti, N. Balucani, *MNRAS* **2013**, *432*, 3423–3430.

37 P. F. Goldsmith, R. Liseau, Tom A. Bell, John H. Black, J.-H. Chen, D. Hollenbach, Michael J. Kaufman, D. Li , D. C. Lis , G. Melnick, D. Neufeld, L. Pagani , R. Snell , A. O. Benz, E. Bergin , S. Bruderer , P. Caselli, E. Caux , P. Encrenaz, E. Falgarone, M. Gerin, J. R. Goicoechea , Å. Hjalmarson , B. Larsson, J. Le Bourlot, F. Le Petit , M. De Luca, Z. Nagy , E. Roueff , A. Sandqvist , F. van der Tak , E. F. van Dishoeck , C. Vastel , S. Viti , Umut Yıldız, Astrophys. J. **2011**, *737*, 96-113. U. A. Yıldız, K. Acharyya, P. F. Goldsmith, E. F. van Dishoeck, G. Melnick, R. Snell, R. Liseau, J.-H. Chen, L. Pagani, E. Bergin, P. Caselli, E. Herbst, L. E. Kristensen, R. Visser, D. C. Lis, M. Gerin, *A&A*, **2013**, *558*, A58.

38 See for instance: (a) S. H. Chung, A. Violi, *Carbon,* **2007**, *45*, 2400–2410; (b) T. S. Totton, D. Chacrabarti, A. J. Misquitta, M. Sander, D. J. Wales, *Comb. Flame,* **2010**, *157*, 909-914; (c) E. K. Yapp, M. Kraft. "Modelling Soot Formation: Model of Particle Formation", in F. Battin-Leclerc, J. M. Simmie, E. Blurock(Eds.), *Cleaner Combustion: Green Energy and Technology* (pp 389–407). Springer London, **2013** (doi:10.1007/978-1-4471-5307-8_15).

39 A. Cuoci, A. Frassoldati, T. Faravelli, E. Ranzi *Comb. Flame* **2009**, *156*, 2010–2022.

40 M. Wartel, J.-F. Pauwels, P. Desgroux, and X. Mercier *J. Phys. Chem. A* **2011**, *115*, 14153–14162.

41 We have recently studied van der Waals complexes and stacking of small aromatic systems at various computational levels: A. Maranzana, A. Indarto, A. Giordana, G. Tonachini, V. Barone, M. Causà, M. Pavone *J. Chem. Phys.* **2013**, *139***,** 244306, 1-16.

42 A. Giordana, A. Maranzana, G. Tonachini, *J. Phys. Chem*. *C*, **2011**, *115*, 1732–1739.

43 A. Giordana, A. Maranzana, G. Tonachini, *J. Phys. Chem. C,* **2011**, *115*, 17237–17251.

44 H. Sabbah, L. Biennier, S. J. Klippenstein, I. R. Sims, B. R. Rowe, *J. Phys. Chem. Lett.* **2010**, *1*, 2962–2967.

45 D. Chen, T. S. Totton, J. W. Akroyd, S. Mosbach, M. Kraft, *Carbon*, **2014**, *67*, 79–91.

46 T. S. Totton, A. J. Misquitta, M. Kraft. *Phys. Chem. Chem. Phys.* **2012**, *14*, 4081-4094.

47 See M. B. Smith, J. March, *March's Advanced Organic Chemistry*, 6th edition, **2007**, Ch 17, p 1553-1558; in particular section 17-35, in which a multistep carbonyl extrusion is depicted.

48 The mole fraction of atomic oxygen, χ_O, under combustion condition can be important, of the order of 10^{-3}. See for instance: (a) R. S. Barlow, G. J. Fiechtner, J.-Y. Chen, *26th Symposium (International) on Combustion, The Combustion Institute,* **1996**, pp. 2199–2205.
(b) A. R.Choudhuria, S. R. Gollahalli, *Internat. J. Hydrogen Energy,* **2004**, *29*, 1293-1302.
(c) K.C. Smyth, J.H. Tjossem, *23rd Symposium of Combustion, The Combustion Institute, Pittsburgh, PA, USA* **1990**, pp. 1829-1837. (d) D. E. Giles, S. Som, S. K. Aggarwal *Fuel,* **2006**, *85,* 1729–1742.
(e) H. Guo, G. J. Smallwood, *International Journal of Thermal Sciences*, **2007**, *46*, 936–943.
In some cases lower mole fraction values were reported. See for instance Table 1 of : C. J. Butler, A.

N. Hayhurst, *Comb. Flame,* **1998**, *115*, 241–252, and: U. Meier, J. Bittner, K. Just. Th. Kohse-Höinghaus, *Symposium (International) on Combustion,* **1989**, *22*, 1887-1896. See also ref. 24, where x_O is reported to vary from very small values up to 10^{-2}.

49 Molar fractions x_i for a number of species i were measured in a series of works by Fei Qi and coworkers, in experiments carried out with different fuel/oxygen/argon flames. In particular, also x_{O_2} is there reported as a function of *z,* the "height above burner" parameter. Ethyne flame: Y. Li, L. Zhang, Z. Tian, T. Yuan, K. Zhang, B. Yang, F. Qi, *Proc. Comb. Ins.,.* **2009**, *32*, 1293–1300. Benzene flame: B. Yang, Y. Li, L. Wei, C. Huang, J. Wang, Z. Tian, R. Yang, L. Sheng, Y. Zhang, F. Qi, *Proc. Comb. Inst.,* **2007**, *31*, 555–563. Toluene flame: Y. Li, L. Zhang, Z. Tian, T. Yuan, J. Wang, B. Yang, F. Qi, *Energy & Fuels,* **2009,** *23,* 1473–1485. Gasoline flame: Y. Li, C. Huang, L. Wei, B. Yang, J. Wang, Z. Tian, T. Zhang, L. Sheng, F. Qi, *Energy & Fuels,* **2007**, *21,* 1931-1941.

50 K. T. Kang, J. Y. Hwang, S. H. Chung, W. Lee *Comb Flame* **1997**, *109,* 266–281.

51 For a recent study of hydroxyl attack on a PAH system, see: D. E. Edwards, D. Y. Zubarev, W. A. Lester, Jr., M. Frenklach *J. Phys. Chem. A* **2014**, *118*, 8606−8613.

52 J. A Pople, P. M. W. Gill, B. G. Johnson, *Chem. Phys. Lett.,* **1992**, *199*, 557-560. H. B. Schlegel, in *Computational Theoretical Organic Chemistry*, ed. I. G. Csizsmadia, R. Daudel, Reidel Publishing Co., Dordrecht, The Netherlands, **1981**, pp. 129-159. H. B. Schlegel, *J. Chem. Phys.,* **1982**, *77*, 3676-3681. H. B. Schlegel, J. S. Binkley, J. A. Pople, *J. Chem. Phys.,* **1984**, *80*, 1976-1981. H. B. Schlegel, *J. Comput. Chem*., **1982**, *3*, 214-218.

53 R. G. Parr, W. Yang, *Density Functional Theory of Atoms and Molecules*, Oxford University Press: New York, **1989**, ch. 3.

54 Y. Zhao, D. G. Truhlar, *Theor. Chem. Acc.,* **2008**, *120*, 215-241.

55 R. Krishnan, J. S. Binkley, R. Seeger, J. A. Pople, *J. Chem. Phys.,* **1980**, *72*, 650-654.

56 D.E. Woon, T. H. Dunning, Jr. *J. Chem. Phys.* **1995**, *103*, 4572-4585. T.H. Dunning *J. Chem. Phys.* **1989**, *90*, 1007-1023.

57 S. Yamanaka, T. Kawakami, K. Nagao, K. Yamaguchi, *Chem. Phys. Lett.,* **1994**, *231*, 25-33. K. Yamaguchi, F. Jensen, A. Dorigo, K. N. Houk, *Chem. Phys. Lett.,* **1988**, *149*, 537-542.
See also: J. Baker, A. Scheiner, J. Andzelm, *Chem. Phys. Lett.,* **1993**, *216*, 380-388. For discussions concerning the effect of spin projection on the performances of DFT methods, see:. J. M. Wittbrodt, H. B. Schlegel, *J. Chem. Phys.*, **1996**, *105*, 6574-6577; E. Goldstein, B. Beno, K. N. Houk, *J. Am. Chem. Soc.,* **1996**, *118*, 6036-6043.

58 Gaussian 09, Revision A.02, M. J. Frisch, G. W. Trucks, H. B. Schlegel, G. E. Scuseria, M. A. Robb, J. R. Cheeseman, G. Scalmani, V. Barone, B. Mennucci, G. A. Petersson, H. Nakatsuji, M. Caricato, X. Li, H. P. Hratchian, A. F. Izmaylov, J. Bloino, G. Zheng, J. L. Sonnenberg, M. Hada, M. Ehara, K. Toyota, R. Fukuda, J. Hasegawa, M. Ishida, T. Nakajima, Y. Honda, O. Kitao, H. Nakai, T. Vreven, J. A. Montgomery, Jr., J. E. Peralta, F. Ogliaro, M. Bearpark, J. J. Heyd, E. Brothers, K. N. Kudin, V. N. Staroverov, R. Kobayashi, J. Normand, K. Raghavachari, A. Rendell, J. C. Burant, S. S. Iyengar, J. Tomasi, M. Cossi, N. Rega, J. M. Millam, M. Klene, J. E. Knox, J. B. Cross, V. Bakken, C. Adamo, J. Jaramillo, R. Gomperts, R. E. Stratmann, O. Yazyev, A. J. Austin, R. Cammi, C. Pomelli, J. W. Ochterski, R. L. Martin, K. Morokuma, V. G. Zakrzewski, G. A. Voth, P. Salvador, J. J. Dannenberg, S. Dapprich, A. D. Daniels, Ö. Farkas, J. B. Foresman, J. V. Ortiz, J. Cioslowski, and D. J. Fox, Gaussian, Inc., Wallingford CT, **2009**.

59 MOLDEN: G. Schaftenaar, J. H. Noordik, *J. Comput.-Aided Mol. Design,* **2000**, *14,* 123-134. (http://www.cmbi.ru.nl/molden/molden.html).

60 The restricted size of pyrene is not expected to greatly affect the chemical aspects under scrutiny (oxidation and growth). Yet, some rigidity of the bridged PAH-like parts might be inclined in some situations to restrain the extent of their interaction (stacking), by keeping the two rigid pyrene-based units too far apart.

61 This study is not exhaustive of all possible reaction pathways, as is currently done to offer quantitative predictions on all the outcomes of a specific reacting system. Thus, the two opposite processes of growth and destruction are not studied in an complete and quantitative way. Recent examples of studies of that kind, by other groups: A. Landera, R. I. Kaiser, A. M. Mebel *J. Chem. Phys.* **2011**, *134*, 024302; da Silva, G.; Trevitt, A. *Phys. Chem. Chem. Phys*. **2011**, *13*, 8940−8952; G. da Silva *J. Phys. Chem. A*, **2014**, *118*, 3967–3972; and also by us: D. Trogolo, A. Maranzana, G. Ghigo, G. Tonachini *J. Phys. Chem. A* **2014**, *118*, 427**−**440.

62 The single reaction steps can be seen more or less as equilibria, depending on temperature. Therefore, to avoid a notation which would classify them as irreversible or reversible steps on the basis of a rather arbitrary boundary, all structures are connected in the Schemes just by line segments.

63 A first attack conducted by dioxygen is significantly more demanding. The addition to position 1 requires for instance to pass a barrier of 34.3 kcal mol^{-1}, and forms an adduct located at 32.6 kcal mol^{-1}. If the initial attack were instead conducted by other reactive radical species as H or HO, for instance, a doublet radical adduct would of course form in lieu of the triplet diradical, but these cases are not explored in the present paper.

64 Though vdW complexes can be thought of as preceding the addition transition structures, and have been defined on the *E* hypersurface for each addition step, the evolving system does not necessarily pass through them, since (a) it could as well find a way to bypass them, as illustrated in the Supporting Information file, Section 2, and (b) their stability drops with increasing temperature.

65 The oxygen atom (a diradical) is known to react with aromatics. See for instance: R. J. Cvetanović *J. Phys. Chem. Ref. Data* **1987**, *16***,** 261-326; J. M. Nicovich, C. A. Gump, A. R. Ravishankara *J. Phys. Chem.* **1982**, *86*, 1684-1690.

66 The initial O attack can take place on different pyrene positions. Considering the ΔE_{ZPE} values, and making reference to the reactants, the barrier is just 0.3 high for position 1, and the adduct is at -25.4 kcal mol^{-1}. If the attack is on position 2, the TS is at +4.7 kcal mol^{-1}, and the adduct at -5.8. If onto position 4, the TS is at +0.2 kcal mol^{-1}, while the adduct is at -22.8 kcal mol^{-1}, thus comparable to the one whose evolution is here considered explicitly.

67 We use **A1**-**A12** labels for the initial transformations which do not involve a mass increase, apart from the first oxygen atom addition. Then **B1**-**B11** for any of the structures from ethyne, oxygen atom, or dioxygen addition. If primed they differ by having only one oxyl radical functionality instead of peroxyl. Finally, **C1**-**C4** entail mass increase through addition of a second PAH.

68 Extrusion, upon temperature rise, of CO (and CO_2) from functionalized PAHs, taken as representative of soot lamellae zones, was compared with Temperature Programmed Desorption (TPD) experiments in a former study by our group: G. Barco, A. Maranzana, G. Ghigo, M. Causà, G. Tonachini, *J. Chem. Phys.,* **2006**, *125*, 184706.

69 From **A10**, a 5-ring closure might in principle open the way to another formyl loss, but it entails a barrier of [37.8/ 39.5/ 44.9] kcal mol^{-1}, and the pathway is consequently less attractive.

70 This trait is illustrated for instance by D_0 values: only 87 kcal mol^{-1} for an aldehydic hydrogen. See M. B. Smith, J. March, *March's Advanced Organic Chemistry*, 6th ed., Wiley-Interscience, **2007**, Ch. 5, Table 5.4.

71 Depending on the combustion environment, some processes might be initiated by NO intervention on intermediates carrying a peroxyl group to transform it into oxyl, and this aspect is of course connected with CO extrusion and loss of mass. However, NO has obviously no role if nitrogen is absent in a specific combustion environment (i.e. no N_2 and no nitrogen in the fuel). Details on how NO operates are presented in the Supporting Information file, Section 4.

72 A similar 5-ring closure in **A9** is not viable, since it requires overcoming a barrier [31.0/32.5/ 37.2] kcal mol^{-1} high. In this case the two triplet unpaired electrons would be in a situation similar to that of the triplet ethene twisted structure, leading to a strained structure.

73 One example of this is the possible product of addition of HCCH (or $^3O_2$) to the localized sp^2 electron site in **A12**. The vinyl substituent in **A12** (s-cis) can first undergo an easy rotation, which entails a free energy barrier of [6.4/ 8.1/ 13.5] kcal mol^{-1}, to expose the said radical site. The s-trans rotamer so obtained is almost at the same free energy of the s-cis, [-13.5/ -19.6/ -35.6] kcal mol^{-1} (it is not shown in Scheme 4). After a first HCCH (or O_2) addition to the top ring, a further pyrene (PAH_2) addition to the resulting high-spin density atom belonging to this pendant is however expected to produce a rather stiff adduct, without an optimal spatial arrangement of the PAH-like parts, because of geometrical constraints. Therefore it is not discussed any further.

74 Epoxidation of PAHs can be of toxicologic interest, being their epoxides (pro)mutagenic or (pro)carcinogenic, because they interact with DNA. Epoxides of structures close to **B8'** have been studied experimentally: see for instance J. N. Pitts, jr, D. M. Lokensgard, P. S. Ripley, K. A. van Cauwenberghe, L. van Vaeck, S. D. Shaffer, A. J. Till, and W. L. Belser, jr *Science* **1980**, 210,1347-1349. Though in that case the functionalization of benzo[a]pyrene was attained by ozonization, not by direct action of the atomic oxygen, O_3 can simply act as an oxygen atom donor (A. Giordana, A. Maranzana, G. Ghigo, M. Causà, G. Tonachini *J. Phys. Chem. A* **2011**, *115*, 470-481).

75 J. Lowe, P. Elvati, A. Violi, 8th U. S. National Combustion Meeting (The Combustion Institute), University of Utah, May 2013, Paper # 070EN-0335. S.-H. Chung *Computational Modeling of Soot Nucleation,* Ph. D. Dissertation, University of Michigan, **2011**: in particular pp 7, 8, 78 and following pages (Chapter 4).

76 P. Elvati, A. Violi, *Proc. Comb. Inst*. **2013**, *34*, 1837-1843 (in particular p 1842).

77 See for instance: C. A. Schuetz, M. Frenklach *Proc. Comb. Inst.* 2002, **29**, 2307-2314. J. D. Herdman, J. H. Miller *J. Phys. Chem. A.* **2008**, *112*, 6249-6256.

78 See for instance: F. Ossler, L. Vallenhag, S. E. Canton, J. B. A. Mitchell, J.-L. Le Garrec, M. Sztucki, S. di Stasio, *Carbon*, **2013**, *51*, 1-19, and H. Wang *Proc. Comb. Inst.* **2011**, *33*, 41–67.